PEL-E-FAN-T

M. Wenk, P. Sanderbrand, D. Brunner, H. Jerzembek, L. Köhler,
TU Dresden, Institut für Luft- und Raumfahrttechnik (ILR), Marschner Straße 32, 01307 Dresden, Deutschland

Abstract

Wildfires pose an increasing threat to humans and wildlife in Europe as climate change further intensifies fire conducive weather, growing the burnt area and economic damage each year. That's why, the DLR Design Challenge 2022 appointed students with the task to design an efficient, economically reasonable, safe, reliable, and quiet fleet of firefighting aircraft on the foundation of a UAM- or RAM- vehicle. The Propellor Driven Electric Firefighting Autonomous VTOL (PEL-E-FAN-T) presents an excellent solution to the task. As a fixed-wing VTOL the aircraft, designed by the team of TU Dresden, combines the cruise flight advantages of a traditional aircraft with the vertical take-off capabilities of a VTOL whilst minimizing danger for human life by operating without a pilot on board. The hybrid-electric powertrain provides a satisfying range while making VTOL capabilities possible in the first place. Utilizing a canard configuration, the concept features high maneuverability. One of the key features is a modular design, providing a significant advantage to a traditional retrofit both economically and in terms of work hours. Additionally, firefighting, cargo, and passenger configurations are possible with one airframe which is also useful in firefighting situations, e.g., evacuating encircled people.

1. INTRODUCTION AND ANALYSIS OF THE STATUS QUO

Wildfires have been increasing in size and frequency in Europe and all over the world due to a surge of fire-conducive weather, a combination of extreme heat and drought, caused by climate change. In addition to damaging the wild flora and fauna in the region and contributing further to climate change by releasing massive amounts of greenhouse gases, it causes high economic losses. The impact of forest fire in the EU between 2000 and 2017 amounts to about 3 billion euros per year (over 54 billion euros collectively) and is projected to increase to over 5 billion a year by 2070-2100 for certain countries [1]. This provides a significant financial incentive to develop a modern aerial firefighting system that is effective and financially reasonable as well as capable to replace current firefighting fleets.

The 2022 DLR Design Challenge is tailored around this problem. The main task is to design a system of firefighting aircraft, capable of dropping 11000 l of water in one fire attack. Taking off from a regional airport (2000 ft above MSL) on a hot day in Europe. In the given scenario the wildfire (1000 ft above MSL) is 75 NM distanced from the airport while the distance between the fire and the nearest water source (2000ft above MSL) is 15 NM. The minimum operational ceiling is 8000 ft above MSL. The goal is to transport as much water to the fire as possible in a 24-hour window.

To potentially replace and enhance current firefighting fleets in Europe, we have to analyze their weaknesses. For example, we can look at the fleet established in the wake of the rescEU program by the European Union. Presently, 12 firefighting airplanes and 1 firefighting helicopter are available for deployment when wildfires demand a joint European effort. There are many aspects of the status quo to look at. First and foremost, they are all manned aerial operations, putting human lives at risk, increasing operational costs, and limiting the operation time to an average of about 12 hours. Additionally, they are not equipped with the technology to efficiently release water since they just drop the water out of a tank.

Furthermore, they lack high maneuverability and require a landing point, implying that they need to return to a base to refill their water and or fuel tank for the next fire attack. Looking at the financial side, the capital and operational costs are extremely high. A new fleet would have to be able to provide better characteristics in the mentioned fields. That is the aim of the presented concept.

2. DESIGN OVERVIEW

2.1. Aircraft Design

PEL-E-FAN-T is designed for firefighting in the safest and most efficient way possible. As a fixed-wing VTOL vehicle, it combines vertical take-off and landing capabilities, necessary for a water intake from small water sources only approachable by helicopters, with horizontal speed and efficiency offered by traditional airplanes. Maximizing reliability and minimizing possible damage by in-flight failures, the concept uses fixed rotors instead of tilt rotors, which have proven to be unreliable in the proximity of water, especially salt water. Furthermore, tilt rotors are not considered due to their high technical complexity, size, and their weight penalty caused by the tilt and variable pitch mechanisms [3]. Exploiting the high specific power of electric motors, they can be mounted inside longitudinal struts in a symmetric manner in relation to the center of gravity resulting in stable vertical flight. Looking at possible arrangements of the propulsion on hybrid-electric aircraft, distributed electric propulsion (DEP) and wing tip propulsion are discussed most often [4]. DEP uses small propellers mounted along the leading edge of the wing, increasing the lift coefficient at low speeds making it possible to reduce the wing size [5] [6]. By using many sources of thrust this concept is very resilient to failure. However, DEP can cause a significant increase in the operational empty weight and increases the complexity of the aircraft considerably [5]. Wing tip propulsion is capable of reducing drag by attenuating the wing tip vortex due to the propeller rotating counter the vortex [7]. This results in a reduction of induced

doi: 10.25967/570601

drag and therefore higher cruise efficiency. Considering these advantages and drawbacks the propellers for horizontal flight are mounted on the wing tips of the aircraft. The horizontal stabilizer is mounted between the struts far away from the fuselage reducing induced drag and improving flight stability as well as control by maximizing the lever of the control surface. The canard configuration further improves maneuverability and the stall behavior of the aircraft. Electric motors are used because of their high specific power, making it possible to place them into the longitudinal struts next to the fuselage as well as on the wing tips. Combining existing and well-proven technologies the PEL-E-FAN-T operates as a UAV minimizing the risk to human life, minimizing operational costs, and being capable of fighting fires 24h a day. The efficiency of the fire attacks is further increased by using a fleet consisting of 10 modular aircraft, having the ability to coordinate in a swarm autonomously while the pilot only has to maneuver critical flight phases such as water drop or water intake. The PEL-E-FAN-T is designed to change Modules rapidly compared to retrofit techniques, which minimizes costs and cuts conversion time massively for off-season use as a cargo drone. By changing Modules one to two hours a fast and tailored response to the fire with a heterogeneous fleet is possible.

BILD 1. front view firefighting configuration

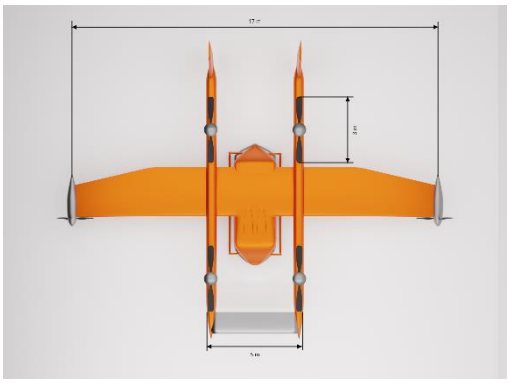

BILD 2. top view firefighting configuration

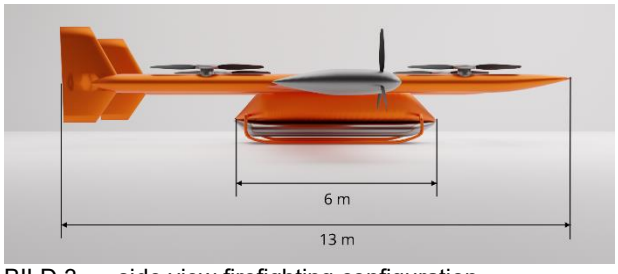

BILD 3. side view firefighting configuration

Technical Data	
MTOW	5679 kg
$L_{aircraft}$	13 m
S_{wing}	17 m
$d_{rotor,VTOL}$	3 m
$d_{rotor,FF}$	2 m
L_{module}	6 m
W_{module}	2 m
V_{water}	1100 l

TAB 1. data overview

2.2. Hybrid-Electric Powertrain

The main drivers behind design decisions regarding the propulsion system of the PEL-E-FAN-T were the maximization of useful load and the minimization of weight. Reducing both environmental and noise pollution was also desired. Optimizing for a greater useful load allowed us to fulfill the mission requirements with a smaller fleet size. This has a major impact on costs and therefore the economic feasibility of the project. Considering the requirements regarding emissions, minimum range, and flight profile, it was determined that these can only be met with the use of hybrid propulsion systems. Electric motors are both relatively light and cheap. They furthermore allow them to be placed as structural components within the airframe, saving both weight and money [8]. Additionally, all-electric motors can be controlled individually, which allows for stable hovering, while taking in water. Hydrogen propulsion was considered but ultimately discarded, because of a lack of hydrogen infrastructure. Exemplary for the low hydrogen coverage, Spain can be used. It only has 120 hydrogen fuel stations, which is insufficient for use in quick emergency service vehicles [9]. That is the reason why the PEL-E-FAN-T is based on a hybrid propulsion system with conventional turbines. This suits the mission profile perfectly. Airbus and Siemens predict that by 2030 it is possible to build passenger aircraft with a capacity of fewer than 100 seats with hybrid propulsion [10]. This shows the potential of hybrid propulsion and the feasibility of operating a hybrid aircraft with our MTOW at EIS. Furthermore, simulations of hybrid-electric propulsion systems suggest that by the EIS of PEL-E-FAN-T, the specific energy density of batteries will be high enough to complete short-haul missions. Since modern aircraft can be expected to have a service life of 30-35 years, hybrid-electric propulsion systems can significantly reduce emissions compared to conventionally powered aircraft [11]. On top of the aforementioned advantages, further reduction of aircraft noise can be achieved through hybrid-electric propulsion. Components that generate the most noise can be positioned in more soundproofed areas. Furthermore, it is possible to reduce the propeller noise by operating at lower rotational speeds by using the high torque of the electric motor [8].
Concerning the technological readiness level, the technology of PEL-E-FAN-T is based on a wide variety of concepts that already exist or are currently under development. Examples of the general configuration are the "ALIA-250c" from Beta Technologies and the "Chaparral" from Elroy Air. In addition, there are various other concepts with electric and hybrid drives, which have a proven TRL between 5 and 7. Examples of this TRL include “E-Fan X” which is being designed in collaboration between Airbus, Rolls Royce, and Siemens and the 9 Passenger aircraft “Alice” engineered by EVIATION [12]. These examples show a wide range of functional deployment options, which

are all in agreement with the given entry into service. This allows us to justify the feasibility of our configuration with a hybrid propulsion

2.2.1. Propulsion

In this configuration, only the electric motors are connected to the propellers. The turbine engine drive generators, which then drive the motors or charge the batteries through a rectifier. During times of low power demand (e.g. cruise flight), the batteries can be recharged, which significantly improves the total range. The simplicity of this system allows for easy propulsion control, which enables the pilot to concentrate on his essential tasks during the firefighting attack. Furthermore, the turbine engine can run constantly at its best operating power and speed [12]. Another advantage of the PEL-E-FAN-T's drive system is that the series hybrid architecture allows a multiple rotor layout, where each propeller has its electric motor [13]. This makes it possible to place the rotors optimally and at the same time, it improves stability during the water intake and flight, because each motor is individually controllable. This allows the pilot to be more responsive to environmental conditions [12].

2.2.2. Power and Energy demand

To estimate the power demand of the aircraft, the air density and aircraft data had to be determined, this is done in other chapters of this paper, and all values and parameters can be found in the appendix. Using the equations 1 to 24 from the paper [14], the power and energy demand will be determined below.
First of all, the power to hover P_{hover} the Aircraft was calculated since it is a critical flight maneuver. The Pump that is used to fill up the aircraft´s water tank, in this segment of the flight, has an approximate power of 5 kW and only needs about 20 s to pump up the 1100 kg of water. This power is very small, less than 0.5 %, in comparison to the power that is needed to hover the aircraft. For these calculations the pump´s power and the energy consumption are negligible.

(1) $$P_{hover} = \frac{W_0}{\eta_{hover}} \cdot \sqrt{\frac{DL}{2 \cdot \rho}}$$

The takeoff power P_{to} is calculated by using P_{hover} and depends on the Rate of climb RoCto and the hover velocity v_h, which is calculated using (16).

(2) $$P_{to} = P_{hover} \cdot [\frac{R_{oCto}}{2 \cdot v_h} + \sqrt{(\frac{R_{oCto}}{2 \cdot v_h})^2 + 1}]$$

After takeoff or starting from hovering the aircraft vertically climbs to the desired height for the transition to take place and does this with R_{oCvcl}. Besides that, the same values as in (2) are being used for this calculation.

(3) $$P_{vcl} = P_{hover} \cdot [\frac{R_{oCvcl}}{2 \cdot v_h} + \sqrt{(\frac{R_{oCvcl}}{2 \cdot v_h})^2 + 1}]$$

Now that the aircraft has reached its desired height and the transition starts. Using the forward propellers the aircraft starts to gain horizontal velocity, but still needs its VTOL motors to produce enough lift that the aircraft does not lose altitude. The required power is the sum of the induced power $P_{induced}$, the power to overcome the drag of the rotor blades $P_{drag,rotor}$ and the power to overcome the drag of the aircraft. To calculate these powers the transition velocity v_{trans} was set and the blade solidity σ was calculated, as well as the speed at the rotor tips v_{tip}. The other terms and coefficients can be found in TAB5.

(4) $$P_{trans,hc} = P_{induced} + P_{drag,rotor} + P_{drag,aircraft}$$

The Aircraft has now reached the transition velocity and goes into the climbing flight. It is estimated that the rate of climb Ro_{Ccl} is constant and can be calculated by the climb angle γ_{climb} and the climbing speed v_{climb} . With this, the power for the climbing flight can be calculated using (5).

(5) $$P_{climb} = \frac{W_0}{\eta_{climb}} \cdot (R_{oCcl} + \frac{v_{climb}}{L_{D,climb}})$$

Following the climb, the aircraft accelerates to cruise speed v_{cruise} and starts its cruise flight, to simplify the calculations all segments of the flight were seen as continuous. The lift to drag ratio $\frac{L}{D_{cruise}}$ and the efficiency coefficient η_{cruise} can be found in TAB 5. As a simplification the power for the descent flight is included in this equation.

(6) $$P_{cruise} = \frac{W_0 \cdot v_{cruise}}{L_{D,cruise} \cdot \eta_{cruise}}$$

As the aircraft prepares for landing or goes into the hovering state, a second transition takes place. The calculations for that are similar to the ones for the first transition(7). The velocity of the second transition was set to be equal to the velocity of the first.

(7) $$P_{trans,ch} = \frac{W_0}{\eta_{trans}} \cdot \sqrt{\frac{-(v_{trans}^2)}{2} + \sqrt{(\frac{v_{trans}^2}{2})^2 + (\frac{W_0}{2 \cdot \rho \cdot A \cdot n_{rotor}})^2}} + \rho \cdot A \cdot v_{tip}^3 \cdot (\frac{\sigma \cdot C_{D,rotor}}{8}) + 0{,}5 \cdot \rho \cdot v_{trans}^3 \cdot C_{D,trans} \cdot S_{wing}$$

Coming to a full stop in midair, the aircraft starts to descend. Here again, already known equations can be used. The calculation of the descending Power is the same as the ones for the vertical climb. Instead of R_{oC}, the rate of descent R_{oD} is used, and caused by the downwards movement, is negative. If the value of R_{oD} is between -2 and 0 the airflow is in a vortex stream state, here the flow is turbulent [15]. An approximation for the induced velocity $v_{i,desc}$ can then be made with (8) going back to an experimental approach by [16].

(8) $$v_{i,desc} = v_h \cdot [k + k_1 \cdot (\frac{R_{oD}}{v_h}) + k_2 \cdot (\frac{R_{oD}}{v_h})^2 + k_3 \cdot (\frac{R_{oD}}{v_h})^3 + k_4 \cdot (\frac{R_{oD}}{v_h})^4]$$

(9) $$P_{vd} = P_{hover} \cdot [\frac{R_{oD}}{v_h} + (\frac{v_{i,desc}}{v_h})]$$

As the aircraft finishes its mission it sets land. The landing power can be calculated using (23) and (10) but instead of R_{oD}, R_{oDld} is applied.

(10) $$P_{ld} = P_{hover} \cdot [\frac{R_{oDld}}{v_h} + (\frac{v_{i,ld}}{v_h})]$$

To simplify the calculations, the MTOW was used as the weight of the aircraft in every stage of the flight. The lift and drag coefficients as well as any other term that is not specifically calculated above can be found TAB 4 With the calculated powers an approximation for the mass of the motor can be made. Assuming the specific power-to-

weight ratio is 10 $\frac{kW}{kg}$, like the Equipemake Ampere-220, the installed electric motor mass m_{eng} can be calculated. For that, it is necessary to use the highest required power, P_{vcl}, and the efficiency of the motors of about 95%.

(11) $$m_{eng,vtol} = \frac{P_{vcl}}{m_{eng,spec} \cdot \eta_{em}}$$

The same method can be applied to estimate the mass of the motors that propel the aircraft forward. The segment with the maximum required power is the climbing flight with P_{climb}.
The power that is demanded to have a R_{oCsc} at the service ceiling can be calculated with the following equation and can be managed with the installed power, where v_{climb} will be generated with a γ_{climb} of 8 instead of 4.

(12) $$v_{climb} = \frac{R_{oCcl}}{\sin(\gamma_{climb})}$$

(13) $$P_{climb,sc} = \frac{W_0}{\eta_{climb}} \cdot (R_{oCcl} + \frac{v_{climb}}{L_{D,climb}})$$

To provide this energy two turbogenerators like the PT6C-67 C were installed. They have a continuous output of 815 kW and takeoff power of 861 kW [19]. In some segments of the flight, this power is not enough and the difference will be provided by the battery. In case one engine fails, the other turbine can produce a total power of up to 1217 kW for 2,5 minutes, and a continuous output of 1064 kW together with the battery it has enough power to fly the aircraft to the nearest airport. Now that the power for each maneuver is determined, the energy demand can be estimated. First, it is necessary to calculate the time the aircraft spends in each segment, by using the velocities and distances [14]. To calculate the total energy, demand the number of firefighting attacks was iteratively defined. Each aircraft fulfills 20 attacks and 19 water intakes. The following equation was used to calculate the individual and the total energy demand.

(14) $$E = P * t$$

The amount of fuel that is needed for this operation is estimated by using the energy density of kerosine and the efficiency of the turbine, which is set to 40% considering the entry into the service year and the fact that future turbines and generators will be optimized for each other.
An example of that is the new Turbogenerator from Rolls Royce [20], a turbine specified to supply electric aircraft with power. This leads to an approximate fuel mass of 933 kg kerosine for 20 attacks. In this mass is a reserve included, enough for a flight of 75 NM and the safe landing of the aircraft.

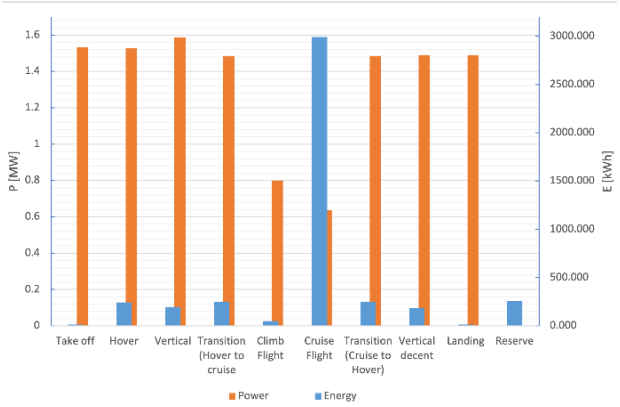

BILD 4. power/energy demands in different flightphases

2.2.3. Battery and system architecture

The PEL-E-FAN-T is designed around a hybrid system consisting of two turbine engines, each powering an electrical generator. The turbogenerators supply the bulk of electrical power needed during a mission to the electric motors. The Battery system of the PEL-E-FAN-T is not designed to act as the sole energy source for the entire flight mission. Instead, it acts as an energy buffer in situations where the demand cannot be satisfied by the turbo generators alone, like during water intake. It, furthermore, stores enough energy to vacate the danger zone and reach a landing spot within a 15 km radius in case of a complete turbine or generator failure.
The following battery characteristics were mainly considered during the design phase:

1) high battery safety
2) high specific energy density
3) sufficient avg. discharge rate (C-Rate)
4) high cycle life/ longevity
5) low cost
6) environmental impact

Lithium-Sulfur Batteries, although not in serial production yet, look most auspicious. They are far superior in terms of safety compared to conventional lithium-ion batteries because their cell chemistry and operating mechanism greatly decrease the risk of catastrophic cell failure. [23] While a thermal runaway event as in Li-Ion cells remains possible, depending on the electrolyte used, the extent of such events is far lower, according to research [23]. The specific energy density of Li-S Batteries is said to increase to 650 Wh/kg by 2030 [24], while the cost is forecasted to be substantially lower than Li-Ion batteries due to much lower material and logistical costs due to their cell stability [25]. The abundance of Sulfur across all areas of the world and its in toxic nature position Li-S cells as an environmentally favorable battery option [26]. Disadvantageous properties of the Li-S battery are their relatively low longevity and low average discharge Rate. The cycle life is said to increase to 1000-2500 cycles until the cell falls short of 80 % of the design capacity [24]. The PEL-E-FAN-T is designed with a specific energy density of 400 Wh/kg in mind. Unfortunately, new Battery systems pushing the boundaries of what is possible regarding energy density are usually poor performers in terms of longevity, C-Rating and reliability. Since the battery system ought to be dependable for many consecutive missions, we chose to take a conservative estimate for battery performance. With this conservative approach, we can ensure that our design is not compromised due to slow battery development.

Data	Unit	Value
Gravimetric energy density	$[\frac{Wh}{kg}]$	400
Volumetric energy density	$[\frac{Wh}{l}]$	300
Total energy	[kWh]	77.6
Weight	[kg]	194
Volume	$[m^3]$	0.259

TAB 1. major battery data

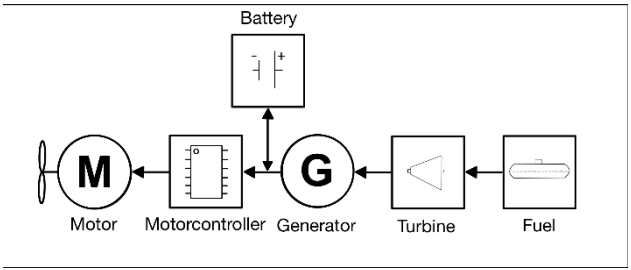

BILD 5. system architecture

2.3. Modules

One of the key features of the PEL-E-FAN-T is the modular design. The mechanism to change Modules is simple and fast to minimize time spent on the ground. All Modules and aircraft have to be equipped with sensors for lining up with the aircraft. A mechanical linking system consisting of a crane in the main aircraft to lift the modules into place as well as fixing points where the modules are safely locked into place. Because those parts can get exposed to sea water, they consist of stainless steel. Additionally, an electrical connection has to be provided for certain modules. To Change modules, the aircraft is positioned in a place where the module can be stored, via ground handling wheels (similar to those for helicopters).
The module is mechanically released and let down by the crane. Then the PEL-E-FAN-T is manually positioned above the desired module, being lined up via sensor feedback. After picking up the module, locking it into place, and potentially manually linking their electronics the aircraft is again ready for take-off. Designing such a system in detail should not prove to be very difficult since companies such as Elroy Air have already implemented similar systems on their cargo drones. In case of switching to a module with different dimensions, the PELE-FAN-T gets jacked up with standardized helicopter lifting jacks at four points on the longitudinal braces to change the skids so the next module will fit beneath the aircraft. To reduce weight and increase efficiency all modules consist of CFRP.

2.3.1. Firefighting Configuration

The most critical module to fulfill the task the “PEL-E-FAN-T” was designed for are the firefighting modules. To minimize flight instabilities from pendulum effects which are difficult to control in a UAV the firefighting module is equipped with a belly tank with a volume of 1100l. To avoid carrying empty mass around, the firefighting module got smaller dimensions. With a width of 1.5, a height of 0.5 and a length of 6 meters it is the smallest among all of them. Covering small and big water sources the module has to be able to function without complications. To take in water as fast as possible from small to large water sources, a hose (diameter 6 inches) with a hover refill pump (450 hp) can be installed, capable of pumping 1500 Gallons per minute (5678.118 l/min) and only weighing in at 100 lbs (45.36kg). These figures are derived from current models by KAWAK AVIATION TECHNOLOGIES. The tank fills up in only 20 seconds. At large accumulations of water (lakes, the sea etc.) scooping is a more efficient way to fill up the water tank. It is within reasonable possibility that a “Sea Snorkel” like the one on the S-64 Helitanker can be installed and used to extend the range of the aircraft since hovering is not necessary. The “Sea Snorkel” could replace the traditional snorkel in suitable circumstances, making it necessary for the module to have a mechanism to easily replace one system with the other. In case of using a fire retardant an additional tank can be implemented into the module for storage. An additional pump will be necessary for rationing the needed volume of chemicals to ensure the perfect mixture of water and fire retardant when dropped onto the fire, which will be provided with the needed electricity through high current cables.

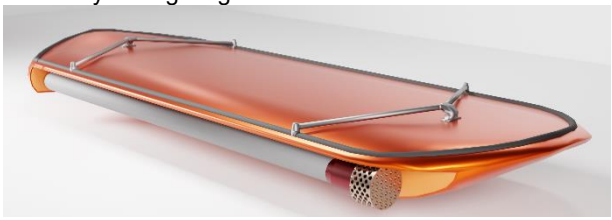

BILD 6. firefighting Module

2.3.2. Cargo Configuration

Similar to the system Elroy air is already using, the PEL-E-FAN-T can function as a cargo drone both in the firefighting season and the off season. With its modular design capability, the aircraft is designed to minimize loading time, maximizing efficiency and income. Additionally, it eliminates piloting costs since the transport of cargo happens fully autonomously, since there are no critical maneuvers (like in the firefighting mission) where a pilot would be needed. The Cargo feature can not only be used in transporting goods between cities but also to haul items to remote areas where infrastructure might be lacking or the access is limited, since the PEL-E-FAN-T has VTOL capabilities and only needs a small area to land. The Cargo module has an aerodynamically improved shape while being flat at the bottom to stand stable on the ground. With a height and width of 2 meters and a length of 6 meters it is designed to fit an LD2 container into it, making transshipment of bigger machinery possible. For loading and unloading the Cargo, a hatch with a width of 1,80 and height of 1,72 meters is located on each side of the module.

BILD 7. cargo configuration

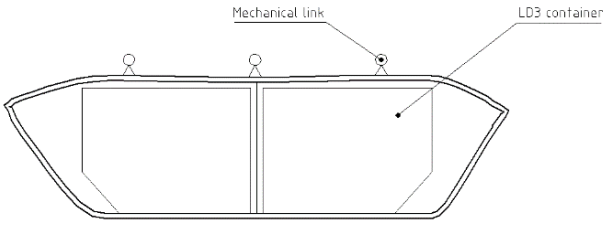

BILD 8. cargo module layout

2.3.3. Evacuation Configuration

Besides the firefighting module being the primarily used configuration during the whole operation, an evacuation module can also be necessary if a person has to be rescued. Therefore, the cargo module can be modified within one to two hours making space for a rescue

stretcher, devices for respiratory monitoring, an emergency backpack, and a seat for a paramedic. To run all the included devices, the module will be provided with the needed electricity through power cables.

2.3.4. Passenger Configuration

During off season, the “PEL-E-FAN-T” can be used in the Urban Air Mobility sector in the passenger configuration. Therefore, a similar module to the cargo with the same dimensions will be used, saving development time. It offers room for up to six passengers and has windows on each side of the cell. The hatch will also be similar to the one used in the cargo module. All the included electrical devices like the lights and the air conditioning will be provided with the needed electricity through high current cables.

2.4. Aerodynamics

2.4.1. Wing

The wing geometry is tailored around the requirements for the aircraft. Flying at subsonic speeds, sweeping the wing is not necessary. Increasing aerodynamic efficiency, the outer sections are tapered providing a reduction in induced drag in comparison to an untampered wing and saving manufacturing costs compared to an elliptical wing. As the Profile of the Wing NACA 4415 has been chosen, providing enough lift in cruise flight to fly with an angle of attack near zero degrees as well as a low sensitivity to different Reynolds numbers in the operating window of the PEL-E-FAN-T as seen BILD 9. To further reduce the stalling speeds triple slotted flaps are installed making it possible to reach a local CL of 3.5 with a deflection angle of about 40° (figure 5 from [27]). This reliable and proven technology enables the PEL-E-FAN-T to reach a low speed of 129.8 km/h. For flight situations where a lower speed is required, the VTOL capabilities of the PEL-E-FAN-T are used.

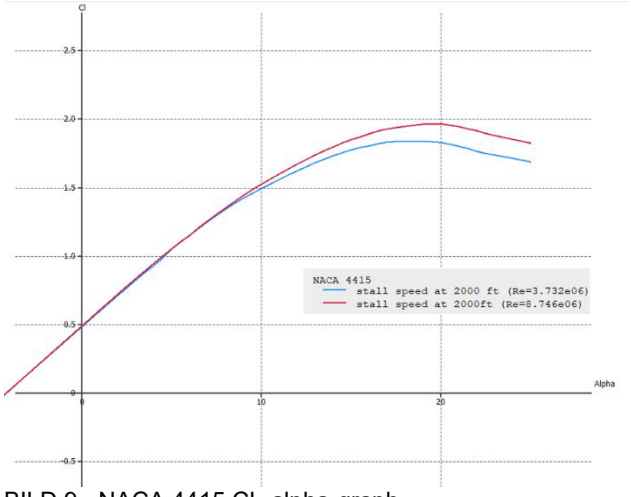

BILD 9. NACA 4415 CL-alpha-graph

2.4.2. Canard and Stabilizer

During a fire attack, the aircraft has to deal with several external influences, such as wind gusts, that can change the flight behavior and therefore the precise fire suppression. The aircraft also has to carry a huge volume of water or chemicals to the source of the fire, which requires a lot of lifting force. The canard configuration of the aircraft provides several advantages that are useful in terms of this demand profile. Its two main purposes are firstly to improve the maneuverability of the aircraft, which is essential in slow flight conditions and secondly to reduce wing loading of the main wing in critical flight situations. Especially the improved maneuverability is essential for the remote-control in-flight phases such as the water drop since the pilot cannot judge critical flight situations as well as he could if he physically sat inside the aircraft. To benefit from the anti-stall characteristics of this configuration the canard has to stall before the main wing avoiding the loss of lift. Benefiting from modern control technology the PEL-E-FAN-T avoids flight stability disadvantages often associated with the canard configuration, allowing the use of relaxed static stability without compromising handling qualities [28]. Sizing the canard, the approximation method for horizontal stabilizers by RAYMER is used (formula 25). Instead of using a tail volume coefficient of 0.1 for the canard described by RAYMER, a more conservative estimation of 0.29 has been chosen to account for possible modifications in further development aiding flight stability. The canard position has to be above or below the main wing and far away from the main wing to reduce the manipulation of the flow around the main wing [29] and at the same time maximizing the moment arm. Therefore, the canard is mounted on the highest point most forward of the struts while the main wing is positioned on the lowest possible point. Mounting it in between the struts also comes with the benefit of a reduction in induced drag as well as less influence of the canard vortex on the main wing. The vertical stabilizer has been positioned at the farthest point aft the main wing to maximize the momentum arm, minimizing its wing area. The sizing follows the approach by RAYMER (formula 26). The results of the sizing of the vertical as well as the horizontal stabilizer can be seen in TAB 2.

	Moment Arm [m]	Area $[m^2]$
Canard	6	4.002
Horizontal Stabilizer	7	5.508

TAB 2. results of stabilizer sizing

2.4.3. Drag estimation

To estimate the zero-lift drag coefficient CD0 of the aircraft, OpenVSP software with a simplified model was used. The firefighting configuration has been used for this estimation. BILD 10 shows the resulting distribution of pressures over the body of the PEL-E-FAN-T.

2.5. Mass

A first accurate analysis of an aircraft’s mass is vital for all further design work. The method applied to obtain the desired approximate mass originates from F. Dorbath, initially published in the Aeronautical Engineering Handbook. In contrast to other methods, Dorbath makes do with less information and was found to yield results similar to or even more accurate than different approaches, all while consistently staying on the conservative side. [30] Furthermore, it allows for a rectangular fuselage and includes optimized formulas for aircraft below 5700kg MTOW. Dorbath is, therefore, best suited for our application. The method divides the aircraft into ten subgroups and approximates the weight of all relevant systems and structures within each group: Wing Mass, Fuselage Mass, Horizontal Tail Plane Mass, Vertical Tail Plane Mass, Landing Gear Mass, Pylon Mass, Power Units Mass, Systems Mass, Operators Items Mass. The unique shape of the fuselage, with its twin-boom design and central

fuselage box, posed a unique challenge during weight analysis. It was solved by adding the volume of the booms to the rectangular fuselage box and calculating the m_{fus} with the resulting increased length. Other approaches like calculating m_{fus} for all three fuselage components separately would have resulted in unacceptable deviations since, as stated previously, formula m_{fus} not only includes the hull structure but all relevant subsystems and structures within the fuselage. These include the cargo hold floor, Paneling, and special structures like a landing gear bay. These subsystems are already accounted for twice due to the separately analyzed module hull structures, and some, like the landing gear bay structure, are not part of PELE-FAN-T. The non-conservative approach to approximating the twin-boom fuselage weight is thereby accounted for. Since PEL-E-FAN-T uses simple skids instead of conventional landing gear, the calculated value for the landing gear was halved. Correction factors for the use of composite structures got applied to the wing and fuselage masses.

2.5.1. Shifting CG

Dealing with shifts in Cg location is of utmost importance for all firefighting aircraft, as during water intake and fire attacks, changes occur rapidly, and water usually slushes during flight. PEL-E-FAN-T, with its canard configuration and multirotor design, is excellently equipped to cope with all these problems. The canard configuration allows for a wider CG range than standard configuration aircraft. Furthermore, to prevent both fuel and water from slushing and endangering the stability of the aircraft, both tanks are compartmentalized. All four vertical engines can be controlled individually. This not only enables VTOL capabilities in the first place but also provides a unique coping mechanism for residual slushing. During water drop, the aircraft can be retrimmed quickly thanks to the canards. The canards are sized larger than necessary for standard aircraft to provide additional maneuverability. The shift in CG location over an entire mission is shown in BILD 10.

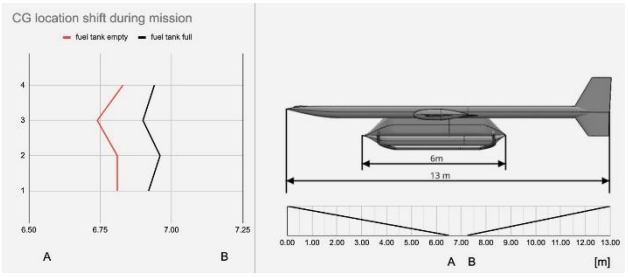

BILD 10. shifting CG

2.5.2. Safety and Failure Modes

Arial firefighting comes with a lot of risks due to dangerous wind conditions, a shifting CG, limited visibility, and multitasking of the pilots leading to human errors. To eliminate the danger to these people the PEL-E-FAN-T is operated remotely and only needs to be manually controlled in critical flight phases, flying autonomously in redundant and predictable situations such as cruise flight, therefore reducing the workload on the pilot. The risk for failure of the required computer systems is negligible due to redundancy. Though a software-based issue can occur, not being able to find a solution to a given problem, and has to be accounted for. In this case, the system switches to remote control to let the pilot handle the situation. In case of the failure of one rotor in a VTOL flight phase the aircraft is capable to stabilize itself using a combination of internal and external sensors [2]. Should a rotor fail in cruise flight then the other horizontal motor is turned off and a combination of gliding and VTOL capabilities are used to land safely. Although capable of withstanding gusty winds, extreme situations have to be accounted for. Therefore, the PEL-E-FAN-T can switch into VTOL mode if stall of flight instability occurs. Should communication with the aircraft not be possible then the aircraft will transition itself into hover mode and find one of the safe locations to land, defined before and updated during the fire attack.

3. AVIONICS AND AUTONOMY

A large percentage of the operating costs of a small aircraft are personal expenses [32]. For many years the number of people operating an aircraft shrunk, whereas the number of electronic assistance systems increased. In the following, two ways of further decreasing the crew costs are described.

3.1. Single Pilot Operation

The first concept is the SPO with only the captain in the aircraft some of the tasks previously done by the Co-Pilot are now carried out by AS and the GO. But still, the PIC has the final decision-making power over the aircraft and delegates tasks to the AS and the ground operator [32]. In the SPO the operating conditions can be divided into four categories, or as it is described in, [32] TC. For that two criteria are important, the pilot condition, either normal or incapacitated, and the flight condition, which is nominal or off-nominal. TC1 is the average operating state and means the pilot`s condition is normal and the flight condition is nominal. When the flight conditions change to off-nominal the operating conditions switch to TC2. Is the pilot incapacitated, meaning he is not able to control the aircraft for example caused by a health issue, and the flight conditions are nominal the operating state is set to TC3. The worst-case scenario would be TC4 where the pilot is incapacitated and the flight conditions are off-nominal. A Dispatcher works in the AOC, where the air traffic is controlled and managed, in the case of an SPO he turns into a GO, the co-pilot on the ground [32]. Supporting the PIC he helps plan the route, checking the list before takeoff, and provides him with information about the air traffic and possible changes in the weather conditions or the mission profile. In TC1 scenarios one GO can work together with up to 20 pilots in different aircraft [32]. But if it comes to an abnormal situation the conditions change to TC2 or higher. In this case, a very high workload must be managed by the pilot, and one-to-one support is needed. In TC3 or 4 a GO takes over the control of the aircraft, which means he must have the possibilities and capabilities to fly this aircraft. Therefore, the GO must be an active pilot and the AOC must have the technical abilities and instruments to radio control an aircraft, it has to be equipped with a second cockpit. To realize the SPO there are two concepts. First of all the hybrid ground operator unit, where one GO is responsible for all tasks, from dispatching to radio-controlled flying of the aircraft, and the special ground unit, where the GO supports the aircraft until, in case of a TC3 or 4, a ground pilot has to step in. One advantage of the SPO is the fact that there is always a pilot on board the aircraft. This leads to better situational awareness and shorter responding times. However, this is also its greatest disadvantage. Since in firefighting scenarios dangerous maneuvers are performed and so human lives are put at

risk. But still, one safety factor is the fact that SPO aircraft can fly partially autonomous and can be remote-controlled. In the end this concept only leads to little savings in the personal sector and having a pilot on board means having a Cockpit, which costs space and mass, limited resources in aviation.

3.2. Autonoumous Flight

An UAS is marked by the fact that there is no operating pilot needed in the air. A part of UAS is an UAV. This UAV can be either remote-controlled or fly autonomously. Many Nations have been using UAVs for many years now, for instance, the MQ9-A „Reaper“ or the RQ-4B „Global Hawk“. Also, Amazon put their first packaging drones to the test [33] and in September 2021 one of the first firefighting UAVs was introduced, the WILD-HOPPER [34].

3.2.1. Hardware

To realize a UAS a series of sensors, that can perform in any weather or light condition, are needed. Like the WILD-HOPPER, PEL-E-FAN-T has two independent navigation systems. On one side it uses Galileo, the European satellite navigation system, which is the most accurate in the world, with a precision of 10-50 cm [35], and on the other side, an IMU is used. In case Galileo should fail, GPS steps into work. An IMU consists of acceleration sensors, gyroscopes, and magnetometers. Using acceleration and rotation data of the aircraft, position and velocity can be calculated. The magnetometer can detect slight changes in the magnetic and gravitational field of the earth, which then can be compared to a map. In some IMUs pressure and temperature sensors were installed, collecting data that can be used to calculate the air density [36]. One technology that is currently used to share the position of the aircraft with others is FLARM. It uses GPS and radio signals to communicate and is very lightweight [37]. To prevent any crashes with obstacles or other aircraft, PEL-E-FAN-T has a variety of distance measuring sensors to detect critical situations or possible crashes as soon as possible. A sensor that is very common in robotics is the sonar. It is the cheapest of these distance measuring sensors but only has a range of several meters [38]. These sensors are used for the autonomous landing of UAVs [39]. With a larger range of 250m and a detection angle of up to 270°[38] LiDAR provides a very accurate but expensive method of measuring distances [40]. To detect other aircraft on a larger scale, radar is being used. It has a range of several kilometers and enables the UAV to detect unknown aircraft and calculate an effective way to change its flight path. To give the GO an image of the situation on-site PEL-E-FAN-T is equipped with several cameras for visible light, this way a 3D image can be produced and distances can be measured, and also the size of the observed object. Such cameras as well as the software are already being used in aircraft [38]. An Infrared camera provides night vision and can be used to detect heat sources, for instance, fires or pockets of embers that usually would not be seen. These high-resolution infrared cameras are used by the police to search for missing or wanted persons [41]. A possible use for the search and rescue configuration of PEL-E-FAN-T. The camera data can not only be used to measure the distance, size, and trajectory of an object but also to calculate the position and speed of the aircraft itself [42]. Comparing images with database landscapes can be recognized, a further way for the UAV to orient itself.

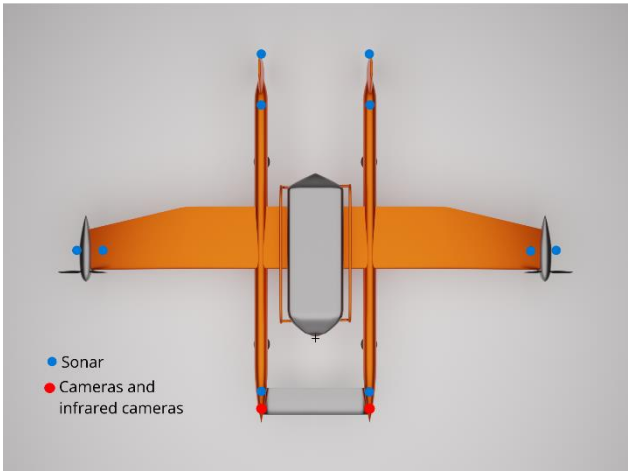

BILD 11. bottom view with sensor positioning

3.2.2. Software

The Data that has been collected must be processed and transferred in a fast and reliable fashion. Then the information is either fed back into the loop of autonomy or given to the operator in a user-friendly way. In [34] programs that were designed for this application were listed, some examples are “Mission Planner, QGround Control, UgCS, Horizon, and others “[34]. Each of them must give the operator intuitive and safe control over the aircraft. One safety feature that is provided by these programs is the "return-home-function“. Once implemented the aircraft will return to the home base or a predefined position, fully autonomous. In case the aircraft loses its connection to the operational base for a longer period, it will automatically implement this program on its own. Small UAVs, such as the DJI Mavic 3, already have this feature and they work reliably [43]. Using the kinetic data, collected by the IMU, PEL-E-FAN-T can fly threw possibly rough weather and wind conditions and keeps a steady course and altitude due to advanced software. To increase the efficiency of the UAS, area maps are provided in a shared cloud and then loaded into each aircraft before each mission. These maps help the UAV orientate itself in known areas. They can be updated by every aircraft and shared among each other [38]. These updates can be temporary, for instance, a foreign aircraft with a certain trajectory has been spotted, or long-term, for example, there is a new building being built. In the firefighting scenario information about water sources and fires can be shared, laying the foundation for a global firefighting strategy. This data is being shared among the fleet, as well as orders and further information provided by the ground control, giving a certain redundancy in case an aircraft loses the global connection for a brief time. UAVs and operators communicate using radio signals and internet links. In the context of this paper, no detailed software will be discussed.

4. OPERATIONAL CONCEPT

4.1. Fleet Size

PEL-E-FAN-T should be used in a homogeneous fleet of 10 aircraft to reach the highest extinguishing effectiveness. The fairly accurate number of ten aircraft is justified by the data arising from a simulation program developed by the DLR [43].

4.2. Fleet type

The concrete air attack then consists of two stages. Two of the ten drones will be deployed initially after the fire became known. Those won't have an extinguishing module attached so their range and airspeed will be increased for faster reconnaissance operations such as discovering small water sources and memorizing the ways to get there. The consequent information will be stored in the chief system of the fleet to enable their access to the remaining drones. Immediately after the required data is provided by the reconnaissance drones, they head back to the operational base and the remaining eight will be deployed with a water module attached. As soon as the scouting drones arrive, they got an extinguishing module attached and immediately head back to the fire. The first fire attack will be finished after they delivered their 2200 liters to fire. The use of a completely homogeneous fleet provides several valuable key benefits for the user such as low material and maintenance costs, which are achieved by uniform testing. Additionally, there are lower storage costs and standardized building plans for the fleet whereby the time and effort of the production can be minimized. Furthermore, there are savings in terms of pilot training, because the control system does not change and they only have to learn one concept. This fact ensures the continuous availability of pilots.

4.3. Ground Handling and General Tactics

For parking and quick launching of our aircraft, it is important to have access to an electric charging station and fuel. Furthermore, a storage area is needed which protects the aircraft from environmental influences. Finally, access to large amounts of water must be guaranteed at all times for filling the water modules. These requirements suggest that the operational base does not necessarily have to be an airport since the takeoff run is not essential due to the VTOL characteristic of our aircraft. Therefore, larger warehouses or other largescale buildings could also be used as a stationing location, which simplifies the wide-area coverage of a forest fire endangered region with firefighting aircraft immensely, due to the resulting shorter distances to the fire.
The key feature of PEL-E-FAN-T's fleet is that the routes between the fire, water resources, and operational base are saved in a chief system simultaneously with the reconnaissance of the location. This makes it possible to put the drones on a kind of autopilot during en-route flights later, which reduces the time of getting controlled by a pilot. This means technically that for ten aircraft no longer ten pilots are needed. In this concept, their tasks are divided into flying firefighting attacks and refueling the modules. In concrete terms, two are supposed to actively extinguish the fire, one should observe the drones during refueling and intervene in case of emergency, and the fourth is a reserve in case the others are overwhelmed. One cycle in the firefighting attack lasts 17 minutes, which means that for ten aircraft, a refueled aircraft arrives every 100 seconds. Thus, one of the two firefighting pilots receives a new drone every 3 minutes and has one minute to drop the water before the next one arrives. Consequently, it is possible to achieve a continuous firefighting operation of 24 hours with a team of 12 pilots and an 8-hour shift system. It should be mentioned that the eight hours are not planned in one piece rather they are distributed over the 24 hours in blocks between 1 and a maximum of 4 hours. Each pilot would have a rest period of 16 hours each day, which is a significant reduction in workload compared to current standards. Another advantage would be the savings in salaries for the pilots since significantly less would be needed.

4.4. Design Missions

4.4.1. Inland Scenario

The PEL-E-FAN-T can operate perfectly in an Inland Scenario because it is designed to use even the smallest lakes for water intake, which makes it very efficient. The Procedure is similar to the one described at Tactics, starting with the deployment of 2 reconnaissance drones.
Those will head directly to the fire source, split up, and circle the affected area transferring the flown route to the central control system. After surrounding the area, the drones will start searching for nearby stretches of water and transmit those coordinates completing the route. Finally, they head back to the operational base where they get equipped with a tank module to complete the fire attack the other eight drones have already performed. The firefighting will be done continuously without interruption due to the pilot's shift system as explained in "Ground Handling". The procedure will always be in accordance with the Design Mission. As a specific example for an Inland Scenario, the fire in Jüterbog in Brandenburg will be looked at. In 2019 the fire broke out in a former military exercise area and quickly spread out, setting 750 hectares of forest and meadow alight. There can be found several smaller lakes not wider than 150 meters in a radius of 10 kilometers around the area, where it won't be possible for conventional air tankers to fill with water. They will have to fly more than twice the range to reach a water source big enough for a scooping maneuver. The PEL-E-FAN-T is perfectly designed to use even the smallest lakes for water intake due to its "pump snorkel" and hover ability, making the firefighting even more efficient. For the sake of simplicity, the drones will start from the Leipzig/Halle airport located 90 kilometers away from the fire, also being able, in case of a longer-lasting firefight, to be stationed at a smaller local airfield, as soon as the needed components were brought there.

4.4.2. Seaside Scenario

The fire in the Costa del Sol tourist area in the Sierra Bermeja Mountain region near Malaga will be used as an example to illustrate the concrete procedure of a firefighting operation. Back in 2021, fires caused devastation there and destroyed 9.000 hectares of forest [48]. This year the area burned again and caused great damage since the area is difficult to access for ground troops due to the heavy vegetation, which makes the use of the PEL-E-FAN-T justifiable. In this case of operation, it might be worth considering the possibility of equipping the area with the small sensors for early detection already mentioned in the point "Ground Handling", since fires rage here almost every year and the danger posed by them can be significantly limited as a result. Furthermore, the pilots will be guaranteed a better view of the fire with a simultaneous immense reduction of the danger and the stress. For simplicity, the drones would be stationed at Malaga Airport, which is just under 100km away from the fire. It is planned that the basic sequence of the firefighting attack is the same as in the design mission, with the water being taken mainly from the Mediterranean Sea, which is only about 10km away. In the direction of the sea, there are several small water sources along the rivers "Arroyo de Enmedio" and

"Arroyo Vaquero", which could be approached by a configuration without "sea-snorkel" and could be made usable as well, which would reduce the distance between water intake and drop even more. In terms of effectiveness, in this scenario, the fleet is heterogeneous in terms of modules. Nevertheless, nothing changes for the pilots' control except that the fourth will have to temporarily intervene due to the increased probability of overload for the remaining three.

4.5. Further Uses

Outside of various firefighting missions, the PEL-E-FAN-T is suitable for agricultural field watering, as an air taxi, for mountain rescue, and as a drone for delivering packages. Because of the extinguishing lance, which is included in the water module, it is possible to extinguish an urban fire in cases where the drone has enough space to maneuver since her wingspan is 17m.

5. COST ESTIMATION

5.1. Life Cycle Cost

Predicting the Lifecycle costs of an aircraft is particularly difficult in times of economic uncertainty. Empirical formulas of a modified DAPCA IV Cost Model, called the Eastlake model, are used [49]. Correction factors for the development of composite aircraft are applied. All calculated costs and salaries are adjusted for inflation. Finally, the engineering, avionics and flight-test operation costs got increased by 100%, 50% and 10%, respectively, to account for the more complex remote-control system, autonomous flight capability and additional testing and development required for the different modules and their systems. Battery prices are projected to be between 200-250$ per kWh [50] [24]. It is assumed that 150 aircraft will be built over a five-year period. With these parameters in mind, one aircraft is expected to cost 15.8 million dollars with a 10% profit margin. The yearly operating costs amount to around 756.100 dollars, assuming a yearly flight time of 1500 hours, and a pilot salary of 150 $/h. The fuel cost is estimated to be around 2.22 $/gal based on the assumption that the increase in fuel cost matches the increase in oil prices stated in an RC-EU-TIMES report [51]. According to this report, the oil price is likely to increase by 46 % from the 2015 level, up until 2030. It
has to be mentioned though, that current fuel prices are much higher. The plane is designed to fly mostly autonomous and requires only minimal attention from an external pilot. One pilot is able to supervise three airplanes at a time, which massively decreases crew costs.

5.2. Impact of Autonomy

High-performance systems lead to increasing costs of purchase, the cheapest way to realize the sensor system would be using cameras [37]. A great part of the costs will be compensated by the sinking personal costs, saving about 75% of the crew. Also, the fact that every firefighting attack is at the same time a reconnaissance flight, leads to a saving of costs for further aircraft and their operation. An AI-based planned route and firefighting will make the PEL-E-FAN-T more effective and efficient [52] [53], giving it even more advantages over conventional firefighting aircraft of this size.

6. CONCLUSION

The challenge provided by the DLR in 2022 to design an efficient, safe, cost-appropriate firefighting aircraft concept can be met by many different designs. However, the PEL-EFAN-T is the optimal solution for a modern aerial firefighting system. The VTOL capabilities combined with the efficiency in cruise flight due to the fixed wing configuration provides the aircraft with a unique package of key advantages compared to current aircraft. Furthermore, the autonomous and remote-control capabilities of the system eliminate the risk for the life of the pilot in dangerous flight maneuvers during the fire attack. Due to modular design the PEL-E-FAN-T offers versatility never seen before opening up new possibilities in firefighting and fire rescue but also provides a fast way to switch to a configuration used for generating profit in the off season, overshadowing initial costs. The PEL-E-FAN-T is more efficient, precise, safe and versatile as well as more profitable than current fleets.

Appendix

i.1 References

[1]*Forest Fires*. url: https://ec.europa.eu/commission/presscorner/detail/e%20n/ip_22_3719.

[2]Sihao Sun et al. “Autonomous quadrotor flight despite rotor failure with onboard visionsensors: Frames vs. events”. In: *IEEE Robotics and Automation Letters* 6.2 (2021), pp. 580–587.

[3]P Nathen et al. *Architectural performance assessment of an electric vertical take-off and landing (e-VTOL) aircraft based on a ducted vectored thrust concept*. 2021.

[4]Julian Hoelzen et al. “Conceptual Design of Operation Strategies for Hybrid Electric Aircraft”. In: *Energies* 11 (Jan. 2018), p. 217. doi: 10.3390/en1101021.

[5]Smruti Sahoo, Xin Zhao, and Konstantinos Kyprianidis. “A Review of Concepts, Benefits, and Challenges for Future Electrical Propulsion-Based Aircraft”. In: *Aerospace* 7.4 (2020). issn: 2226-4310. url: https://www.mdpi.com/2226-4310/7/4/44.

[6]Mark D Moore. “Distributed electric propulsion (DEP) aircraft”. In: *NASA Langley Research Center* (2012).

[7]Tomas Sinnige et al. “Wingtip-Mounted Propellers: Aerodynamic Analysis of Interaction Effects and Comparison with Conventional Layout”. In: *Journal of Aircraft* 56(Nov. 2018), pp. 1–18. doi: 10.2514/1.C034978.

[8]Dr. Andreas Klöckner. “Die Zukunft fliegt elektrisch! Vom Lufttaxi bis zum Regionaljet”. In: *LUFTFAHRT – Elektrisches Fliegen* (). url: https://www.dlr.de/content/de/downloads/2017/die- zukunft-fliegt-elektrisch.pdf?__blob=publicationFile&v=4.

[9]glpautogas.info. *wasserstoff tankstellen in spanien auf Juli 2022*. 2022. url: https://www.glpautogas.info/de/wasserstoff-tankstellen-spanien.html.

[10]V. G. Volchenko and A. N. Ser’yoznov. “Hybrid and electric propulsion system of aircrafts”. In: *AIP Conference Proceedings* 2351.1 (2021), p. 030015. doi: 10.1063/5.0052622. eprint: https://aip.scitation.org/doi/pdf/10.1063/5.0052622. url: https://aip.scitation.org/doi/abs/10.1063/5.0052622.

[11]Gabrielle E. Wroblewski and Phillip J. Ansell. “Mission Analysis and Emissions for Conventional and Hybrid-Electric Commercial Transport Aircraft”. In: *Journal of Aircraft* 56.3 (2019), pp. 1200–1213. doi: 10.2514/1.C035070. eprint: https://doi.org/10.2514/1.C035070. url: https://doi.org/10.2514/1.C035070.

[12]Manuel A. Sánchez R. Carlos D. Gallo M. Josselyn Anzai Alexandre H. Rendón. “Aircraft Hybrid-Electric Propulsion: Development Trends, Challenges and Opportunities”. In: *Journal of Control, Automation and Electrical Systems* (). url: https://doi.org/10.1007/s40313-021-00740-x.

[13]J.Ludowicy R.Rings D.F.Finger C.Braun. “Sizing studies of light aircraft with serial hybrid propulsion systems”. In: *Deutscher Luft- und Raumfahrtkongress 2018* (). url: https://www.dglr.de/publikationen/2018/480226.pdf.

[14]Michael Schultz Robert Brühl Hartmut Fricke. “Air taxi flight performance modeling and application”. In: *2021* ().

[15]Constantin Rotaru and Michael Todorov. “Chapter 2 Helicopter Flight Physics”. In:2018.

[16]J. G. Leishman. “Principles of Helicopter Aerodynamics”. In: *2000* ().

[17]Equipmake. “Data Sheet Ampere-220”. In: *2022* ().

[18]Jae-Hyun An et al. “Advanced Sizing Methodology for a Multi-Mode eVTOL UAV Powered by a Hydrogen Fuel Cell and Battery”. In: *Aerospace* 9.2 (2022). issn: 2226-4310. url: https://www.mdpi.com/2226-4310/9/2/71.

[19]EASA. “TYPE-CERTIFICATE DATA SHEET PrattWhitneyCanada PT6C-67 series engines”. In: (2012).

[20]*Rolls-Royce unveils its new ’turbogenerator’ with a new small engine*. url: https://interestingengineering.com/rolls-royce-turbogenerator-engine.

[21]CAL FIRE. “Firefighting Aircraft Recognition Guide”. In: *2019* ().

[22]Global Helicopter Service GmbH. “AIRCRAFT SPECIFICATION SHEET BELL 212- D-HEPP”. In: (2022).

[23]Xueyan Huang et al. “Comprehensive evaluation of safety performance and failure mechanism analysis for lithium sulfur pouch cells”. In: *Energy Storage Materials* 30 (2020), pp. 87–97. issn: 2405-8297. doi: https://doi.org/10.1016/j.ensm.2020.04.035. url: https://www.sciencedirect.com/science/article/pii/S240582972030163X.

[24]C. Pornet and A.T. Isikveren. “Conceptual design of hybrid-electric transport aircraft”.In: *Progress in Aerospace Sciences* 79 (2015), pp. 114–135. issn: 0376-0421. doi: https://doi.org/10.1016/j.paerosci.2015.09.002. url: https://www.sciencedirect.com/science/article/pii/S0376042115300130.

[25]Chen Yang et al. “Approaching energy-dense and cost-effective lithium–sulfur batteries: From materials chemistry and price considerations”. In: *Energy* 201 (2020), p. 117718.issn: 0360-5442. doi:https://doi.org/10.1016/j.energy.2020.117718. url:https://www.sciencedirect.com/science/article/pii/S0360544220308252.

*[26]*Abbas Fotouhi et al. *Lithium-Sulfur Battery Technology Readiness and Applications—A Review*. 2017. doi: 10 . 3390 / en10121937. url: https://www.mdpi.com/1996-1073/10/12/1937.

*[27]*Egbert Torenbeek. “Airplane weight and balance”. In: *Synthesis of Subsonic Airplane Design: An introduction to the preliminary design of subsonic general aviation and transport aircraft, with emphasis on layout, aerodynamic design, propulsion and performance*.Dordrecht: Springer Netherlands, 1982, pp. 263–302. doi: 10.1007/978-94-017-3202-4_8. url: https://doi.org/10.1007/978-94-017-3202-4_8.

*[28]*Seth B Anderson. “A look at handling qualities of canard configurations”. In: *Journal of Guidance, Control, and Dynamics* 10.2 (1987), pp. 129–138.

[29]Eugene L Tu. “Vortex-wing interaction of a close-coupled canard configuration”. In: *Journal of aircraft* 31.2 (1994), pp. 314–321.

[30]Arlind Pape. *Analyse der neuen LTH-Methode zur Massenschätzung von Flugzeugbaugruppen*. 2019. doi: 10.7910/DVN/VIOW4X. url: https://dataverse.harvard.edu/citation?persistentId=doi:10.7910/DVN/VIOW4X.

[31]Karl D Bilimoria, Walter W Johnson, and Paul C Schutte. “Conceptual framework for single pilot operations”. In: *Proceedings of the international conference on humancomputer interaction in aerospace*. 2014.

[32]*Amazon darf Drohnenzustellung testen*. url: https://www.tagesschau.de/wirtschaft/amazon-drohnen-101.html.

[33]Ahmed Refaat Ragab et al. “WILD HOPPER Prototype for Forest Firefighting”. In: *International Journal of Online and Biomedical Engineering (iJOE)* 17.09 (2021), pp. 148–168. doi: 10.3991/ijoe.v17i09.25205. url: https://online-journals.org/index.php/i-joe/article/view/25205.

[34]*Mehr Genauigkeit, mehr Altagsnutzung: Galileo*. url: https://www.dlr-innospace.de/innospaceexpo/M&K/Home/content/satellit.html.

[35]*IMU und Robotertechnik: Was Sie wissen sollten*. url: https://www.generationrobots.com/blog/de/imu-und-robotertechnik-was-sie-wissen-sollten-2/.

[36]FLARM. “Kollisionswarnungen und Verkehrsanzeigen für die Allgemeine Luftfahrt und Drohnen”. In: *2020* ().

[37]Franz Andert. “Bildbasierte Umgebungserkennung für autonomes Fliegen”. In: *DLRForschungsbericht 2011-09* (Mar. 2011).

[38]Srikanth Saripalli, Gaurav S Sukhatme, and James F Montgomery. “An experimental study of the autonomous helicopter landing problem”. In: *Experimental Robotics VIII*. Springer, 2003, pp. 466–475.

[39]*Die wichtigsten LiDAR-Parameter – Den Durchblick behalten*. url: https://www.blickfeld.com/de/blog/lidar-parameter-verstehen/#Detection-Range.

[40]*Modernster Hubschrauber der Welt: Alarmhubschrauber H145*. url: https://polizei.nrw/artikel/modernster-hubschrauber-der-welt-alarmhubschrauber-h145.

[41]Eike Harm Otto Bremers. “Multi-Sensor Data Fusion zur optischen Navigation im Kontext unbemannter Luftfahrzeuge”. In: *2020* ().

[42]*Mavic 3 Imaging Above Everything*. url: https://www.dji.com/de/mavic-3?site=brandsite&from=nav.

[43]Prajwal Shiva Prakasha et al. “Exploration of Aerial Firefighting Fleet Effectiveness and Cost by System of Systems Simulations”. In: *32nd Congress of the International Council of Aeronautical Sciences*. ICAS 2021. International Council of Aeronautical Sciences, 2021. url: https://elib.dlr.de/148125/.

[44]Hofmann Felix Kaulfuß Susanne. “Arten und Strategien der Waldbrandbekämpfung”. In: *Strategien der Waldbrandbekämpfung* (). url: http://www.waldwissen.net.

[45]Prajwal S. Prakasha et al. “System of Systems Simulation driven Urban Air Mobility Vehicle Design”. In: *AIAA AVIATION 2021 FORUM*. doi: 10.2514/6.2021-3200. eprint: https://arc.aiaa.org/doi/pdf/10.2514/6.2021- 3200. url: https://arc.aiaa.org/doi/abs/10.2514/6.2021-3200.

[46]*Professionelle Ausrüstung für Feuerwehren zur Waldbrandbekämpfung*. url: https://www.vallfirest.com/de/frontline.

[47]*Spanien: Waldbrand an der Costa del Sol – 3000 Menschen evakuiert*. url: https://www.stern.de/panorama/spanien--waldbrand- an- der- costa- del- sol---3000-menschen-evakuiert-31935876.html.

[48]Snorri Gudmundsson. *General aviation aircraft design : applied methods and procedures- [1st ed.]* Oxford, UK: Butterworth-Heinemann, 2014. Chap. 2.

[49]Björn Nykvist and Måns Nilsson. “Rapidly falling costs of battery packs for electric vehicles”. In: *Nature Climate Change* 5 (Mar. 2015), pp. 329–332. doi: 10 . 1038 /nclimate2564.

[50]Neven Duić Nedeljko Štefanić Zoran Lulić Goran Krajačić Tomislav Pukšec Tomislav Novosel. “EU28 fuel prices for 2015 2030 and 2050”. In: *2017* ().

[51]Kristian Korsvold Fettig. *Entwicklung einer optimierten Flugbahnplanungsmethode zum Zweck der Flugbereichsbestimmung für unbemannte Luftfahrzeuge*. Tech. rep. Institut für Flugsystemtechnik, Sept. 2020. url: https://elib.dlr.de/139523/.

[52]Moritz Plingen. “Künstliche Intelligenz im Luftverkehr”. In: *2021* ().

[53]KAVAKAVIATION. “Medium Bell 28VDC High Output Hover Refill Pump”. In: *2022* ().

i.2 Formulas

[15] $$DL = \frac{W_0}{n_{rotor} \cdot 2A}$$

[16] $$v_h = \sqrt{\frac{W_0}{2 \cdot \rho \cdot A}}$$

[17] $$\sigma = \frac{N_{rotorblades} \cdot c_{rotor}}{\pi \cdot \frac{(d_{rotor,vtol})^2}{4}}$$

[18] $$v_{tip} = \frac{\pi \cdot RPM \cdot d_{rotor}}{60}$$

[19] $$P_{induced} = \frac{W_0}{\eta_{trans}} \cdot \sqrt{\frac{-(v_{trans}^2)}{2} + \sqrt{(\frac{v_{trans}^2}{2})^2 + (\frac{W_0}{2 \cdot \rho \cdot A \cdot n_{rotor}})^2}}$$

[20] $$P_{drag,rotor} = \rho \cdot A \cdot v_{tip}^3 \cdot (\frac{\sigma \cdot C_{D,rotor}}{8})$$

[21] $$P_{drag,aircraft} = 0{,}5 \cdot \rho \cdot v_{trans}^3 \cdot C_{D,trans} \cdot S_{wing}$$

[22] $$R_{oCcl} = v_{climb} \cdot \sin(\gamma_{climb})$$

[23] $$v_{i,ld} = v_h \cdot [k + k_1 \cdot (\frac{R_{oDld}}{v_h}) + k_2 \cdot (\frac{R_{oDld}}{v_h})^2 + k_3 \cdot (\frac{R_{oDld}}{v_h})^3 + k_4 \cdot (\frac{R_{oDld}}{v_h})^4]$$

[24] $$m_{eng,ff} = \frac{P_{climb,sc}}{m_{eng,spec} \cdot \eta_{em}}$$

[25] $$S_{VT} = \frac{c_{VT} \cdot b \cdot S_{Wing}}{L_{VT}}$$

[26] $$S_{HT} = \frac{c_{HT} \cdot \bar{C}_W \cdot S_{Wimg}}{L_{HT}}$$

[27] $$m_{wing} = 2.20013 \cdot 10^{-4}[401.146 \cdot S_{wing}^{1.31} + MTOW^{1.1038}] \cdot (\frac{T}{C})^{-0.5} \cdot AR^{1.5} \cdot \frac{1}{cos(\phi_{25})}$$

[28] $$m_{fus} = 12.7(l_{fus} \cdot d_{fus})^{1.2982} \cdot (1 - [-0.008(\frac{l_{fus}}{d_{fus}})^2 + 0.1664(\frac{l_{fus}}{d_{fus}}) - 0.8501]) \cdot \frac{w_{fus}}{d_{fus}}$$

[29] $$d_{fus} = \frac{h_{fus} + w_{fus}}{2}$$

[30] $$m_{htp} = 12.908 \cdot S_{HT}^{1.1868}(1 + \frac{0.1 - (\frac{T}{C})}{(\frac{T}{C})})$$

[31] $$m_{vtp} = 25.056 \cdot S_{VT}^{1.0033}$$

[32] $$m_{pylon} = n_{PPT} \cdot 0.0131 \cdot SLST^{0.8806}$$

[33] $$m_{sys} = 42.059(l_{fus} \cdot d_{fus})^{0.9414}$$

[34] $$m_{fur} = 200 + 3.35(l_{fus} \cdot d_{fus})^{1.3368}$$

[35] $$m_{opp} = 35.782 \cdot n_{PAX}^{1.1141}$$

[36] $$m_{land} = 1.8 \cdot 10^{-3} \cdot MTOW^{1.278}$$

i.3 Nomenclature

Abbreviations

AOC	Airline-Operating Center
AS	Assistant Systems
CO_2	Carbon Dioxide
CG	Center of Gravity
ClF	Climbing Flight
CrF	Cruise Flight
DL	Disc Loading
EM	Electric motor
EIS	Entry Into Service
EASA	European Union Aviation Safety Agency
GO	Ground Operator
HO	Hover Flight
IMU	Internal Measurement Unit
ISA	International Standard Atmosphere
L	Landing
L/D	Lift-to-Drag
PIC	Pilot in Command
R	Reserve
RPM	Rotations per Minute
SPO	Single Pilot Operation
TC	Taxonomy of operating Conditions
TRL	Technology Readiness Level
TO	Take Off
TE	Total Energy
Tch	Transition cruise to hover
Thc	Transition hover to cruise
UAV	Unmanned Aerial Vehicle
UAS	Unmanned Aircraft System
VC	Vertical Climb
VD	Vertical Descent

Symbol	Description	Unit
S_{HT}	area horizontal tail	$[m^2]$
S_{VT}	area vertical tail	$[m^2]$
v_{climb}	climb velocity	$[\frac{m}{s}]$
$v_{climb,sc}$	climb velocity service ceiling	$[\frac{m}{s}]$
t_{climb}	climb time	$[s]$
P_{climb}	climb power	$[MW]$
$P_{climb,sc}$	climb power service ceiling	$[MW]$
k	constant for induced velocity	[-]
k_1	constant for induced velocity	[-]
k_2	constant for induced velocity	[-]
k_3	constant for induced velocity	[-]
k_3	constant for induced velocity	[-]
P_{cruise}	cruise power	$[MW]$
v_{cruise}	cruise velocity	$[\frac{m}{s}]$
$v_{descent}$	descent velocity	$[\frac{m}{s}]$
v_d	descent velocity in transition	$[\frac{m}{s}]$
C_D	drag coefficient	[-]
$E_{density,battery}$	energy density battery	$[\frac{Wh}{kg}]$
$E_{density,kersion}$	energy density kerosin	$[\frac{kWh}{kg}]$
$m_{eng,ff}$	engine mass for forward flight	$[kg]$
$m_{eng,vtol}$	engine mass for vtol	$[kg]$
t_{fillup}	fillup time	$[s]$
d_{fus}	diameter fuselage	[m]
m_{fus}	fuselage mass for aircraft, cargo and water module	[kg]
g	gravitational acceleration	$[\frac{m}{s^2}]$
W_0	gravitational force	$[N]$
H	height	$[mm]$
h_{fus}	height of fuselage	[m]
H_{base}	height of the operational Base above Sea Level	$[m]$
H_w	height of the water reservoir above Sea Level	$[m]$
H_{sc}	height service ceiling	$[m]$
c_{HT}	horizontal tail volume coefficient	[-]
P_{hover}	hover power	$[MW]$
t_{hover}	hover time	$[s]$
v_h	induced velocity	$[\frac{m}{s}]$
$v_{i,desc}$	induced vertical descent velocity	$[\frac{m}{s}]$
$v_{i,ld}$	induced vertical landing velocity	$[\frac{m}{s}]$
m_{land}	landing gear mass	[kg]
s_{land}	landing distance	[m]
L	length	$[mm]$
l_{fus}	length of fuselage	[m]
C_L	lift coefficient	[-]
$\Delta C_{\mathrm{a,max,hld,to}}$	lift coefficient triple slotted flap with slotted leading edge flap, take off	[-]
$C_{\mathrm{a,max,hld,l}}$	lift coefficient triple slotted flap with slotted leading edge flap, landing	[-]
$C_{L\alpha}$	lift gradient	[-]
$\frac{L}{D}_{cruise}$	lift to drag ratio in cruise flight	[-]
m_{htp}	mass horizontal stabilizer	[kg]
m_{pylon}	mass engine pylon	[kg]
m_{sys}	mass for electrical system and avionics	[kg]
m_{fur}	mass interior fittings (cargo floor etc.)	[kg]
m_{vtp}	mass vertical stabilizer	[kg]
$MTOW$	maximum take-off weight	$[kg]$
W_{module}	module width	[m]
L_{HT}	momentum arm horizontal tail	[m]
L_{VT}	momentum arm vertical tail	[m]
n_{attack}	number of attacks	[-]
$N_{rotorblades}$	number of rotor blades	[-]
n_{rotor}	number of rotors VTOL	[-]
N_{rotor}	number of rotors cruise flight	[-]
n_{ppt}	number of turbines	[-]
H_{OL}	operational level	$[m]$
m_{op}	operational mass	[kg]
n_{PAX}	number of passengers	[-]
$P_{drag,aircraft}$	power to compensate drag, aircraft	$[MW]$
$P_{drag,rotor}$	power to compensate drag, rotor	$[MW]$
P_{pump}	pump power	$[kW]$
m_{pump}	pump weight	$[kg]$
R_oC_{to}	rate of climbe take off	$[\frac{m}{s}]$
R_oC_{vcl}	rate of vertical climbe take off	$[\frac{m}{s}]$
R_oD	rate of descent	$[\frac{m}{s}]$
R_oD_{ld}	rate of descent landing	$[\frac{m}{s}]$
A	rotor area	$[m^2]$

c_{rotor}	rotor blade depth	$[m]$
$d_{rotor,VTOL}$	rotor diameter VTOL	$[m]$
$d_{rotor,FF}$	rotor diameter forward flight	$[m]$
H_{SL}	sea level	$[m]$
H_{SC}	service ceiling	$[m]$
R	specific gas constant	$[\frac{J}{kgK}]$
$m_{eng,spec}$	specific power density electric engine	$[\frac{kW}{kg}]$
v_{sl}	stalling velocity in landing	$[\frac{m}{s}]$
v_{sto}	stalling velocity in take off	$[\frac{m}{s}]$
$SLST$	statistical combined engine thrust	[N]
s_{start}	starting distance	[m]
E_{to}	take off energy	$[kWh]$
P_{to}	take off power	$[MW]$
t_{to}	take off time	$[s]$
T	temperature	$[K]$
$\frac{T}{C}$	thickness to chord ratio of wing profils	[-]
t_{wf}	time between water reservoir and fire	$[s]$
t_{cruise}	time in cruise flight	$[s]$
t_{base}	time in cruise flight between base and fire	$[s]$
v_{tip}	tip velocity of rotor blades (for VTOL)	$[\frac{m}{s}]$
t_{trans}	transition time	$[s]$
P_{trans}	transition power	$[MW]$
$P_{trans,ch}$	transition power from cruise to hover flight	$[MW]$
$P_{trans,hc}$	transition power from hover to cruise flight	$[MW]$
v_{trans}	transition velocity	$[\frac{m}{s}]$
$m_{turbine}$	turbine weight	$[kg]$
P_{vd}	vertical descent power	$[MW]$
P_{ld}	vertical landing power	$[MW]$
c_{VT}	vertical tail volume coefficient	[-]
t_{fillup}	water fillup time	$[s]$
m_{water}	water weight	$[kg]$
W	width	$[mm]$
w_{fus}	width of fuselage	[m]
S_{wing}	wing area	[m^2]
l_m	wing depth	$[m]$
W_L	wing load	$[kPa]$
m_{wing}	wing mass	[kg]
$\bar{C_W}$	wing mean chord	$[m]$
b	wingspan	$[m]$
C_{D0}	zero drag coefficient	[-]
C_L	zero lift coefficient	[-]

Greek

α	angle of attack	[°]
Λ	aspect ratio	[-]
γ_{climb}	climbing angle	[°]
ρ	density	$[\frac{kg}{m^3}]$
$\eta_{turbine}$	efficiency turbine	[-]
η_{climb}	propulsive efficiency climb	[-]
η_{cruise}	propulsive efficiency cruise	[-]
η_{em}	propulsive efficiency electric engine	[-]
η_{hover}	propulsive efficiency hovering	[-]
$\eta_{prop,ff}$	propulsive efficiency propellor forward flight	[-]
η_{trans}	propulsive efficiency transition	[-]
ρ_{engine}	specific energy density of engine	$[\frac{kW}{kg}]$
$\rho_{generator}$	specific energy density of generator	$[\frac{kW}{kg}]$
$\rho_{kerosin}$	specific energy density of kerosin	$[\frac{kWh}{kg}]$
ϕ	sweep	[°]
λ	taper ratio	[-]
γ_H	temperature gradient	$[\frac{K}{m}]$
θ_{tilt}	tilt angle	[°]

i.4 Additional Tables

	TO	HO	VC	Thc	ClF	CrF	Tch	VD	L	R	TE
t_{total}[s]	30	570	444	600	222	16960	600	444	30	-	19870
P [kW]	1533	1527	1587	1485	800	635	1485	1490	1489	-	-
E [kWh]	12.8	241.7	195.8	247.0	49.4	2991.0	247.0	184.0	12.4	305.4	4487.7

TAB 3. calculated mission energy
(3.2.2 Power and Energy demand)

Data	Unit	Value
MTOW	[kg]	5670
W_0	[kN]	55.604
Λ	[-]	9.9497
d_{rotor}	[m]	3
c_{rotor}	[m]	0.2
n_{rotor}	[-]	4
N_{rotor}	[-]	2
RPM	$[\frac{1}{s}]$	$1.893 \cdot 10^3$
A	$[m^2]$	3.142
S_{wing}	$[m^2]$	30.43
l_m	[m]	2
W_L	[kPa]	1,827
b	[m]	17
v_{sto}	$[\frac{m}{s}]$	35.159
v_{sl}	$[\frac{m}{s}]$	30.675
H_w	[m]	609.6
H_{sc}	[m]	2438
ρ (H_w)	$[\frac{kg}{m^3}]$	1.159
n_{attack}	[-]	20
t_{fillup}	[s]	30
P_{pump}	[kW]	50
$m_{eng,spec}$	$[\frac{kW}{kg}]$	10
$E_{density,kersion}$	$[\frac{kWh}{kg}]$	11.9
s_{start}	[m]	0
$s_{landing}$	[m]	0

TAB 4. aircraft and mission data

Constant	Value	Unit
e	0.77	[-]
c_{rotor}	0.2	[m]
k_d	0.44	[-]
α_{max}	12	[°]
γ_{climb}	4	[°]
S_{ratio}	1.35	[-]
$\Delta c_{a,max,hld,to}$	2.55	[-]
$\Delta c_{a,max,hld,l}$	3.35	[-]
η_{hover}	0.75	[-]
η_{em}	0.95	[-]
η_{climb}	0.73	[-]
η_{cruise}	0.7	[-]
$\eta_{prop,ff}$	0.85	[-]
η_{trans}	0.7	[-]
η_{PT6T}	0.3	[-]
R_{oDld}	-0.5	$[\frac{m}{s}]$
R_{oD}	-4.5	$[\frac{m}{s}]$
R_{oCto}	0.5	$[\frac{m}{s}]$
R_{oCvcl}	4.5	$[\frac{m}{s}]$
R_{oCcl}	4.5	$[\frac{m}{s}]$
R_{oCsc}	0.5	$[\frac{m}{s}]$
k	0.974	[-]
k_1	-1.125	[-]
k_2	-1.372	[-]
k_3	-1.718	[-]
k_4	-0.655	[-]
v_{trans}	60	$[\frac{m}{s}]$
v_{cruise}	75	$[\frac{m}{s}]$
C_{L0}	0.2043	[-]
$C_{L\alpha}$	0.09538	[-]
C_{D0}	0.0176	[-]
$C_{L,climb}$	0.277	[-]
$C_{D,climb}$	0.021	[-]
$C_{D,rotor}$	0.01	[-]
$L_{D,climb}$	13.213	[-]
$L_{D,cruise}$	12.578	[-]

TAB 5. costants for calculation (2.2.2 Power and Energy demand)

Data	Value	Unit
v_{tip}	297.407	$[\frac{m}{s}]$
v_h	58.246	$[\frac{m}{s}]$
$v_{i,desc}$	61.362	$[\frac{m}{s}]$
v_{climb}	64.51	$[\frac{m}{s}]$
$v_{i,ld}$	57.288	$[\frac{m}{s}]$
P_{hover}	1.527	[MW]
P_{to}	1.533	[MW]
P_{vcl}	1.587	[MW]
P_{vd}	1.49	[MW]
P_{climb}	0.8	[MW]
P_{ld}	1.489	[MW]
$P_{induced}$	1.094	[MW]
P_{drag}	0.091	[MW]
$P_{drag,aircraft}$	0.299	[MW]
$P_{trans,hc}$	1.485	[MW]
$P_{trans,ch}$	1.485	[MW]
P_{cruise}	0.635	[MW]
$P_{climb,sc}$	1.209	[MW]
A	7.069	$[m^2]$
DL	0.983	[kPa]
σ	0.34	[-]
E_{to}	12.8	[kWh]
E_{hover}	241.7	[kWh]
E_{vc}	195.8	[kWh]
$E_{trans,hc}$	247.0	[kWh]
E_{climb}	49.4	[kWh]
E_{cruise}	2991.0	[kWh]
$E_{trans,ch}$	247.0	[kWh]
E_{vd}	184.0	[kWh]
E_{ld}	12.4	[kWh]
$E_{reserve}$	305.4	[kWh]
m_{eng}	186.986	[kg]
$m_{eng,vtol}$	202	[kg]
$m_{eng,ff}$	130	[kg]
m_{fuel}	727.589	[kg]

TAB 6. results of calculation (2.2.2 Power and Energy demand)

Subsystem	Data basis	Weigth [kg]
Main Aircraft without modules		
wing mass	formula 27	668.25
fuselage mass	formula 28	501.69
horizontal tail plane mass	formula 30	50.175
vertical tail plane mass	formula 31	124.9
landing gear mass	formula 36	56.4
pylon mass	formula 32	175
power units mass (EM+turbine)	mass estimated from datasheet [17] [19]	662
systems mass	formula 33	332.79
Cargo Module		
fuselage mass	formula 28	409
furnishing mass	formula 34	240.30
Water Module		
fuselage mass	formula 28	319.15
pump module	mass estimated from datasheet [53]	45
Battery		
total mass	calculated with equations of [15]	194
Generator		
total mass	2 MW at 7.66 $\frac{kW}{kg}$	326.4

TAB 7. results of mass calculation (2.5 Mass)

i.5 Additional Graphs

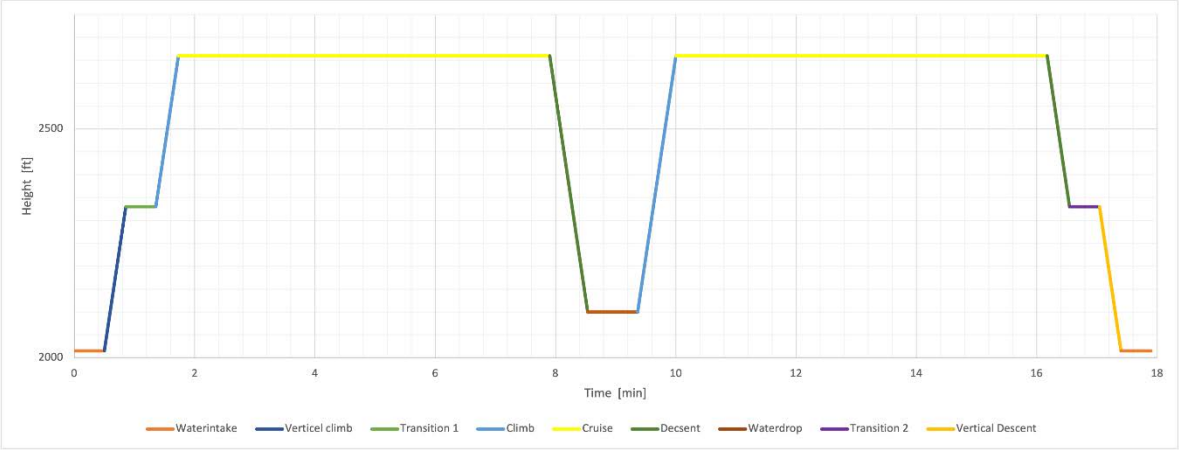

BILD 12. flight phases of the mission profile

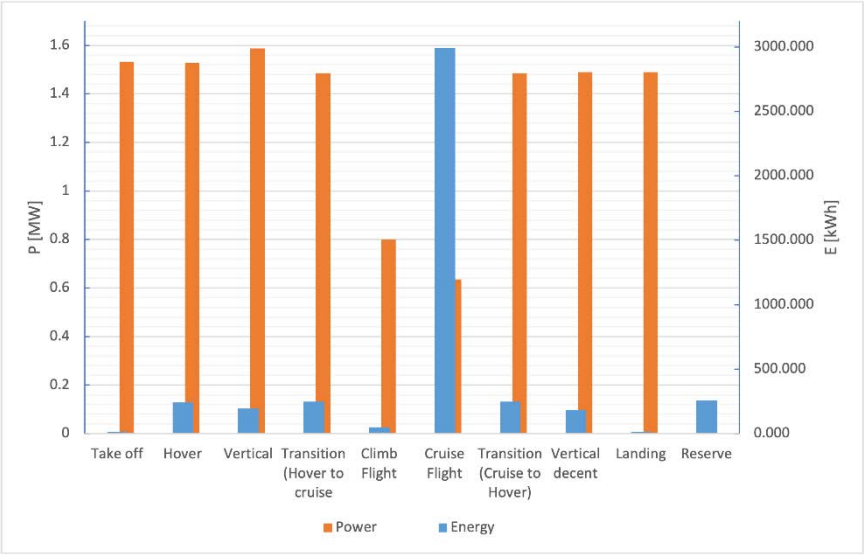

BILD 13. energy requiered in each flight phase

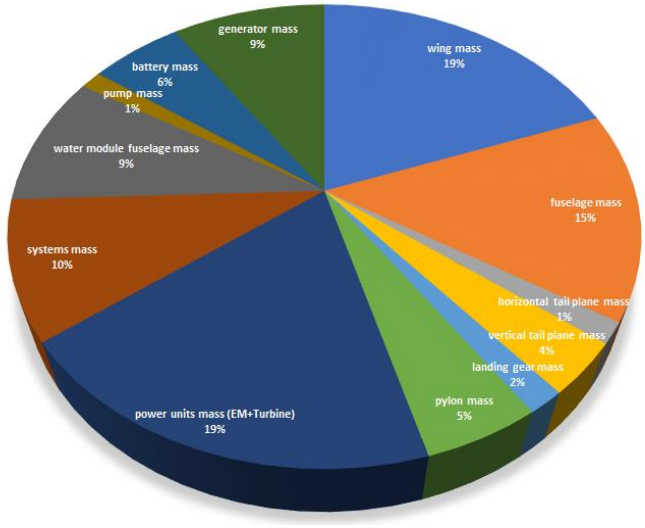

BILD 14. aircraft weight allocation
(OEW 3456 kg)